Author(s): Sulignano, B.; Theisen, Ch; Delaroche, J.-P.; Girod, M.; Ljungvall, J.; Ackermann, D.; Antalic, S.; Dorvaux, Olivier; Drouart, A.; Gall, Benoit; Görgen, Andreas; Greenlees, Paul; Hauschild, Karl; Herzberg, Rolf-Dietmar; Hessberger, Fritz Peter; Jakobsson, Ulrika; Jones, Peter; Julin, Rauno; Juutinen, Sakari; Ketelhut, Steffen; Korten, Wolfram; Leino, Matti; Lopez-Martens, Araceli; Nyman, Markus; Obertelli, A.; Pakarinen, Janne; Papadakis, P.; Parr, E.; Peura, Pauli; Piot, J.; Rahkila, Panu; Rostron, P.; Ruotsalainen,

Title: Investigation of high-K states in 252No

Year: 2012

Version:

Please cite the original version:

Sulignano, B., Theisen, C., Delaroche, J.-P., Girod, M., Ljungvall, J., Ackermann, D., Antalic, S., Dorvaux, O., Drouart, A., Gall, B., Görgen, A., Greenlees, P., Hauschild, K., Herzberg, R.-D., Hessberger, F. P., Jakobsson, U., Jones, P., Julin, R., Juutinen, S., . . . Zielinska, M. (2012). Investigation of high-K states in 252No. Physical Review C, 86(4), Article 044318. https://doi.org/10.1103/PhysRevC.86.044318

Investigation of high-K states in ^{252}No

B. Sulignano,[1] Ch. Theisen,[1] J.-P. Delaroche,[2] M. Girod,[2] J. Ljungvall,[3] D. Ackermann,[4,5] S. Antalic,[6] O. Dorvaux,[7] A. Drouart,[1] B. Gall,[7] A. Görgen,[8] P. T. Greenlees,[9] K. Hauschild,[3] R.-D. Herzberg,[10] F. P. Heßberger,[4,5] U. Jakobsson,[9] P. Jones,[9] R. Julin,[9] S. Juutinen,[9] S. Ketelhut,[9] W. Korten,[1] M. Leino,[9] A. Lopez-Martens,[3] M. Nyman,[9] A. Obertelli,[1] J. Pakarinen,[11] P. Papadakis,[10] E. Parr,[10] P. Peura,[9] J. Piot,[7] P. Rahkila,[9] D. Rostron,[10] P. Ruotsalainen,[9] J. Sarén,[9] C. Scholey,[9] J. Sorri,[9] J. Uusitalo,[9] M. Venhart,[12,6] and M. Zielińska[1]

[1]*CEA, Centre de Saclay, IRFU/Service de Physique Nucléaire, F-91191 Gif-sur-Yvette, France*
[2]*CEA, DAM, DIF, F-91297 Arpajon, France*
[3]*CSNSM, IN2P3-CNRS, F-91405 Orsay Campus, France*
[4]*GSI Helmholtzzentrum für Schwerionenforschung, D-64291 Darmstadt, Germany*
[5]*Helmholtz Institut Mainz, D-55099 Mainz, Germany*
[6]*Department of Physics and Biophysics, Comenius University, Bratislava 842 48, Slovakia*
[7]*Institut Pluridisciplinaire Hubert Curien, F-67037 Strasbourg, France*
[8]*SAFE Kjemibygningen, Sem Sælandsvei 26, 0371 Oslo, Norway*
[9]*Department of Physics, University of Jyväskylä, FIN-40014 Jyväskylä, Finland*
[10]*Department of Physics, University of Liverpool, Liverpool L69 7ZE, United Kingdom*
[11]*Isolde, CERN*
[12]*Institute of Physics, Slovak Academy of Sciences, Bratislava 845 11, Slovakia*

(Received 3 April 2012; revised manuscript received 19 July 2012; published 16 October 2012)

In this paper we investigate the rotational band built upon a two-quasiparticle 8^- isomeric state of ^{252}No up to spin $I^\pi = 22^-$. The excited states of the band were populated with the ^{206}Pb(^{48}Ca, $2n$) fusion-evaporation reaction. An unambiguous assignment of the structure of the 8^- isomer as a $7/2^+[624]_\nu \otimes 9/2^-[734]_\nu$ configuration has been made on the basis of purely experimental data. Comparisons with triaxial self-consistent Hartree-Fock-Bogoliubov calculations using the D1S force and breaking time-reversal as well as z-signature symmetries are performed. These predictions are in agreement with present measurements. Mean-field calculations extended to similar states in ^{250}Fm support the interpretation of the same two-neutron quasiparticle structure as the bandhead in both $N = 150$ isotones.

DOI: 10.1103/PhysRevC.86.044318 PACS number(s): 21.10.−k, 23.20.Lv, 23.35.+g, 27.90.+b

I. INTRODUCTION

In the past few decades exhaustive investigations of deformed nuclei in the transfermium region around $N = 152$ and $Z = 100$, where enhanced stability is observed, have been performed using in-beam and decay spectroscopy [1]. Nuclei in this region are produced with cross sections ranging from nanobarns to microbarns, high enough for detailed spectroscopic studies. Moreover, this region is characterized by the presence of K isomerism, which may enhance the stability of such nuclei against spontaneous fission [2], as in ^{270}Ds [3], in ^{254}No [4], and in ^{250}No [5].

K isomers are due to the presence near the Fermi surface of either neutron or proton orbitals with a large angular momentum projection K along the symmetry axis. Excitation of particles into such an orbital leads to a K state for which the decay is strongly hindered according to the ΔK selection rule. Therefore these states with a strong signature represent a new prolific ground for experimental investigations. The study of K isomers and collective bands built on them provides a detailed probe of single-particle states and their coupling to the collective degrees of freedom. Famous examples are located around $Z = 72$, $N = 106$ and include the textbook example of the $K^\pi = 16^+$ isomer in ^{178}Hf with a half-life of 31 yr (see for instance the review articles [6–8]). In the same way, the investigations of the nobelium isotopes ($Z = 102$), thus, deliver data in a region close to the domain of superheavy nuclei, where our knowledge of single-particle spectra and of pairing correlations is particularly limited. These studies can provide information relevant for the next shell closure, which is expected to be at $Z = 114$, 120, or 126 and $N = 184$ for spherical superheavy elements depending on the model (see [9–11] and references therein).

Ghiorso *et al*. were the first to discover K isomers in this region 39 years ago in ^{250}Fm and ^{254}No [12]. The decay of ^{254}No was recently revisited by Herzberg *et al*. [13] and by Tandel *et al*. [14], where a second isomer was found. In the nucleus ^{252}No, a new K isomer with a half-life of 110 ± 10 ms at an excitation energy of 1254 keV was discovered at SHIP (GSI, Darmstadt) [15] and confirmed at FMA (Argonne National Laboratory) [16], both experiments using decay spectroscopy techniques.

The isomer in ^{252}No has been interpreted as a two-quasineutron state with the configuration $7/2^+[624]_\nu \otimes 9/2^-[734]_\nu$ with spin and parity $I^\pi = 8^-$. This assignment was made by analogy with other $N = 150$ isotones. In fact, $K^\pi = 8^-$ isomers have been found in ^{244}Pu [16,17], ^{246}Cm [16,18], ^{248}Cf [19], and ^{250}Fm [20]. Very similar level schemes are observed in ^{246}Cm and ^{250}Fm, where the $I^\pi = 8^-$ isomer decays into the ground-state rotational bands via an intermediate excited band.

According to previous calculations, using Hartree-Fock-Bogoliubov (HFB) mean-field calculations with the Gogny

D1S force [21], the two-quasineutron $K^\pi = 8^-$ excitation in ^{252}No was predicted to lie at 1070 keV (without breaking time-reversal symmetry in the mean field [22]), in agreement with the experimental excitation energy $E_x = 1254$ keV. This result is in agreement with HFB calculations using the SLy4 interaction, which predict the two-quasineutron $K^\pi = 8^-$ excitation at ∼1300 keV [23]. On the other hand, both HFB models predict the two-quasiproton states at higher excitation energies (i.e., $E_x \sim 2000$ keV). In contrast, the macroscopic-microscopic Woods-Saxon calculations predict $K^\pi = 8^-$ isomers at ∼1 MeV for both two-quasineutron and two-quasiproton configurations [2,16,20]. Recent random phase approximation (RPA) calculations predict a two-neutron quasiparticle state at 1300 keV [24]. The differences between these predictions are related to different single-particle level schemes underlying the models.

The goal of this work is to deduce the structure of the $K^\pi = 8^-$ isomer in ^{252}No with purely experimental data and to understand how this structure changes with the rotational frequency. Together with previous data on ^{250}Fm [20], this will provide valuable reference points for theoretical models.

Strong constraints on the configuration assignment and models is provided (for $K^\pi \neq 0$ states) by the magnetic moment or gyromagnetic factor, which can be determined by measuring the $M1/E2$ intensity ratio within the band. While the $K^\pi = 8^-$ isomer in ^{252}No has been investigated using decay spectroscopy, this work extends the study to a rotational band built above this state via in-beam γ-ray spectroscopy, allowing for firm configuration assignments of the 8^- isomer.

II. EXPERIMENT

The experiment was carried out at the Accelerator Laboratory of the University of Jyväskylä. A $^{48}Ca^{+10}$ beam, with an energy of 218 MeV and an average current of 30 pnA, impinged on 452 μg/cm^2 thick ^{206}PbS (with an enrichment of 98.6%) targets mounted on a rotating wheel. The fusion-evaporation residues were selected by the gas-filled separator RITU [25] and implanted into the focal plane spectrometer GREAT [26]. GREAT consists of a multi-wire proportional counter (MWPC) to measure the time of flight and energy loss ΔE of the incoming ions and double-sided silicon strip detectors (DSSSD) to measure the energy and time of the ions and subsequent decays. The DSSSD are surrounded by germanium detectors (clover and planar) and PIN diodes for the detection of γ rays and conversion electrons from the decay of the implanted recoil. Prompt γ rays were detected in the 41 Compton-suppressed germanium detectors of the JUROGAM array. A γ-ray efficiency of 4.2% at 1332 keV was determined using calibration sources. The JUROGAM detector preamplifier signals were digitized with TNT2 digital pulse processor units [27]. This allowed a counting rate of up to 35 kHz for each germanium detector while retaining good energy and time resolution. Compared to standard analog shaping amplifiers and peak-sensing analog-to-digital converters (ADCs), the use of digital electronics allowed an increase of the average beam current by approximately a factor of 2. A time-stamped system total data readout (TDR) data acquisition system was used [28]. Data analysis was carried out using the GRAIN software package [29].

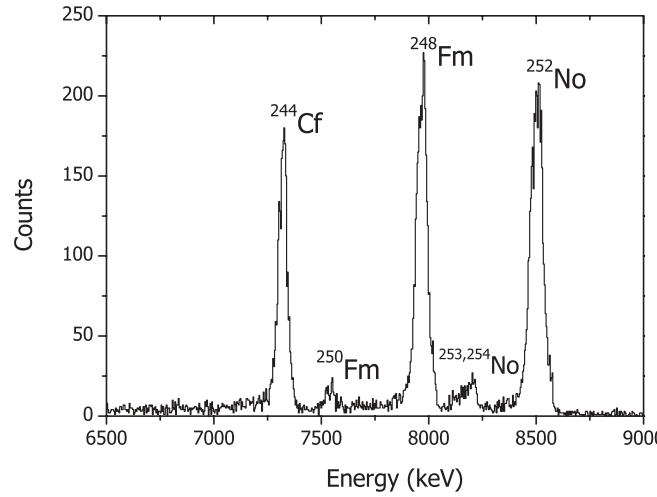

FIG. 1. Energy spectrum of α particles detected at the focal plane.

A total of 198 h of irradiation yielded 1.5×10^4 recoils detected at the focal plane correlated with the decay of ^{252}No and/or its daughters. The identification of the recoils was performed by demanding a signal (ΔE) in the MWPC detector in coincidence with an energy signal in the double-sided silicon strip implantation detector. Correlations between the time of flight and total energy were used to discriminate against scattered beam and target-like reaction products. The lifetime of the ^{252}No ground state was determined by correlating evaporation residues (ERs) with the subsequent alpha decay (α) or spontaneous fission (SF). Since the gain of the silicon detector electronics was optimized for the evaporation residues, events rendering overflow in the energy ADC and in anticoincidences with the MWPC were identified as SF events. The measured branching ratios for the different decay modes of the ^{252}No ground state, namely, $b_\alpha = 65.3(5)\%$ and $b_{SF} = 33.9(3)\%$, are found to be in good agreement with the literature values [30]. The electron capture decay path could not be measured directly so the previously measured value of $b_\epsilon = 0.8\%$ [31] was assumed. The α-particle energy spectrum in anticoincidence with MWPC events is shown in Fig. 1. From the time distribution a half-life of 2.43 ± 0.13 s was obtained for the ground state, in agreement with the evaluated data of 2.44 ± 0.04 s [32].

A. Delayed spectroscopy

Isomeric states in heavy nuclei often decay to the ground-state band via strongly converted electromagnetic transitions. Correlating such electrons, detected in the DSSSD and identified via their energy, with the implanted ERs allows selection of the recoils which were implanted prior to the decay of the isomeric state. For details see, e.g., Jones [33]. The measured electron sum signals of the isomer decays detected in the same pixel as an ER event within a time window of 700 ms after the implantation are shown in Fig. 2. The insert in Fig. 2 shows the logarithm of the time difference between implantation of the recoil and its subsequent electron

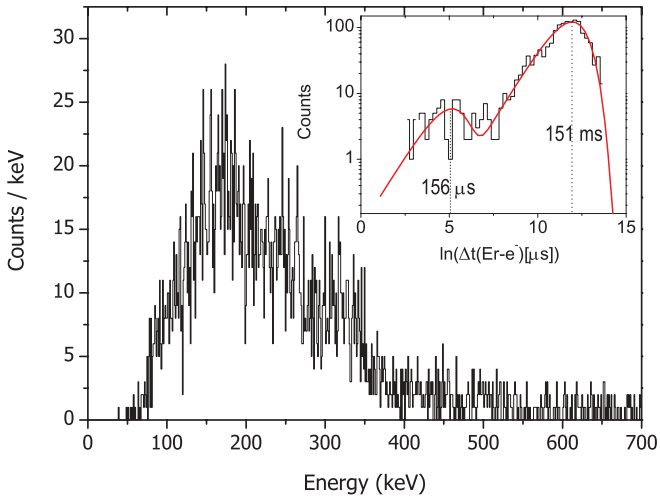

FIG. 2. (Color online) Energy spectrum of conversion electrons observed within 700 ms after a fusion-evaporation residue was implanted in the same pixel of the DSSSD. The inset shows the logarithmic decay time distribution of conversion electrons correlated with ER recoils detected at the focal plane; no correlation with α decay or SF of ^{252}No is required. The smaller contribution at 156 μs is ascribed to a short-lived isomer in ^{253}No.

decay. The red curve represents the time density distribution of electrons correlated to the evaporation residue of ^{252}No, and the peak position determines the lifetime via the $\ln(\tau)$ relation. This method [34,35] allows the discrimination of contributions from sources having different lifetimes. The distinct cluster with a lifetime of 156 μs corresponds most likely to the de-excitation of an isomeric state in ^{253}No. This is confirmed by the observation of the characteristic x rays of nobelium and few γ rays with energies similar to that reported recently by Antalic *et al.* [36]. ^{253}No nuclei have been produced via the $2n$ evaporation channel from reactions on the ^{207}Pb contaminant present in the ^{206}Pb target. The α decay of this channel is also visible in Fig. 1.

For an unambiguous identification and to remove the contribution from ^{253}No, an additional requirement of α decay or SF of ^{252}No observed subsequently in the same pixel was demanded. We should point out that among all possible open channels, ^{252}No is the only nucleus having a SF branch; SF is therefore an unambiguous signature of this nucleus. A total of 3833 conversion electrons (ER-e^- correlation) signals were detected in the DSSSD. A half-life of 109 $\pm$ 3 ms was found, in perfect agreement with 110 $\pm$ 10 ms quoted in [15].

Delayed γ rays from the de-excitation of isomeric states were detected in the germanium detectors surrounding the focal plane. A coincidence with the conversion electrons from the decay of the isomeric state using the conditions 2 ms $<$ Δt(ER-e^-) $<$ 700 ms and $E_e^- < 700$ keV was demanded. See Fig. 3 for the γ-ray spectra. The deduced decay pattern from the isomeric state is found to be in perfect agreement with the previous measurements [15], as shown in Fig. 4.

Moreover, it was possible to confirm the transitions observed in earlier experiments. Indeed, the $6^- \rightarrow 5^-$ (75 keV) $M1$ transition is clearly visible in Fig. 3, as are the $5^- \rightarrow 3^-$ at 107 keV, $7^- \rightarrow 5^-$ at 156 keV, $6^- \rightarrow 4^-$ at 133 keV, and

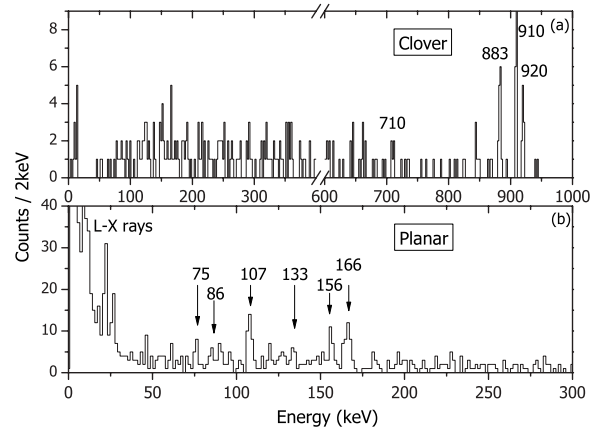

FIG. 3. Gamma rays detected in prompt coincidence with conversion electrons in the clover detector (a) and in the planar germanium detector (b) of the GREAT spectrometer.

$4^- \rightarrow 2^-$ at 86 keV $E2$ transitions. Other peaks are also visible in the spectra, although at present status it is not possible to fit them into our decay scheme.

B. Prompt spectroscopy at the target position

The de-excitation of states lying above the isomer was studied [see Fig. 5(a)] by correlating prompt γ rays in the

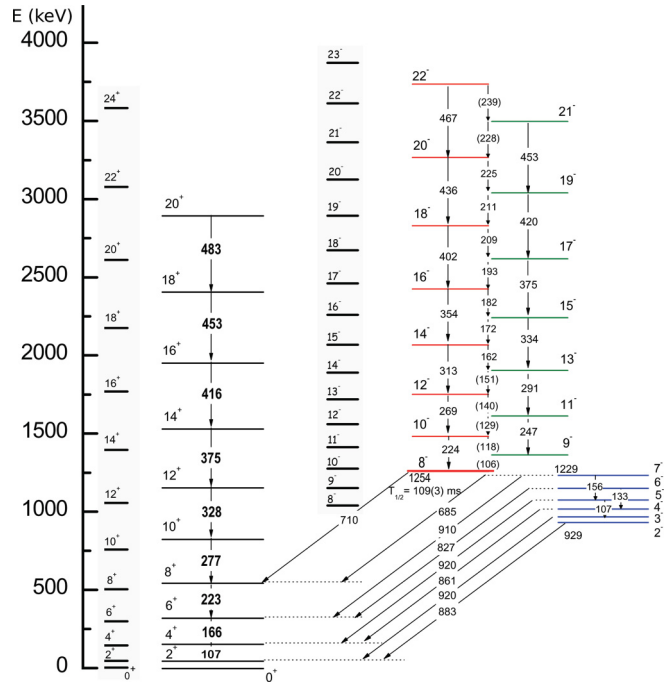

FIG. 4. (Color online) ^{252}No level scheme. Ground-state band measured up to spin $I^\pi = 20^+$ and comparison to HFB predictions to spin 24^+ (gray box) are shown on the left-hand side. The rotational band measured on top of the $K^\pi = 8^-$ neutron isomer is shown (up to spin $I^\pi = 22^-$) in red and green colors for even and odd spin sequences, respectively. HFB level predictions for this band to spin $I^\pi = 23^-$ are shown inside the gray box. The $K^\pi = 2^-$ collective band observed at lower excitation energy is marked in blue.

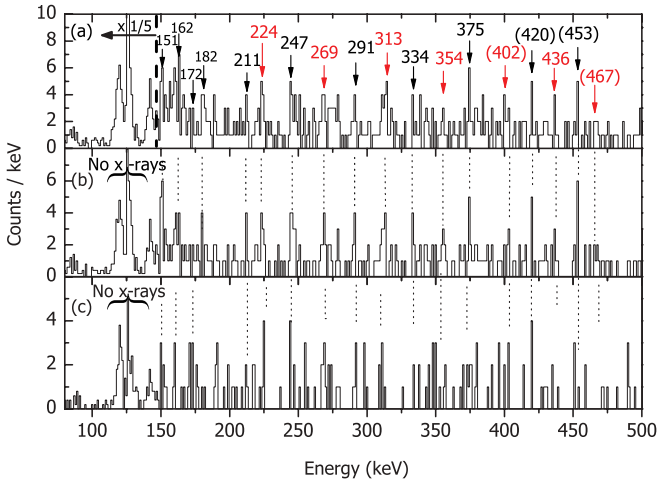

FIG. 5. (Color online) (a) Prompt γ-rays measured in JUROGAM in coincidence with an ER-e^- ($E_{e^-} < 700$ keV) pair observed at the same position in the DSSSD within 700 ms. (b) Same spectrum with the additional requirement that an α particle or SF is correlated with the evaporation residue. (c) Projection of the γ-γ coincidences matrix using electrons and α/SF correlations. The region of nobelium x rays has been scaled down by a factor of 5 in all three spectra.

JUROGAM array with fusion-evaporation residues observed in the focal plane of RITU. The additional requirement that an electron sum event was observed within 700 ms after a recoil at the same position in the DSSSD was made. Higher selectivity was reached by detecting the characteristic α or SF decay following the evaporation residue within ΔT(ER–α/SF) < 12 s [see Fig. 5(b)]. Support for the assignment of the rotational band is given by the investigation of recoil-gated γ-γ coincidences. Figure 5(c) shows the projection of the recoil-gated γ-γ coincidence matrix using electrons and α/SF correlations. Although the statistics are rather weak, each (presumed) transition is in coincidence with at least one of the other transitions. The corresponding level scheme including also transitions from previous work [15,37] is shown in Fig. 4.

C. Spin assignment

The spin I of the states in the rotational band built on top of the isomer can be assigned using a method extensively applied to superdeformed rotational bands in the mass 190 region [38,39]. The technique known as the Harris fit [40] consists in expanding the dynamic moment of inertia $\mathcal{J}^{(2)}$ in even powers of the rotational frequency $\hbar\omega = E_\gamma/2$ averaged over two consecutive γ-ray transitions,

$$\mathcal{J}^{(2)} = 4/\Delta E_\gamma = dI/d\omega = A + B\omega^2 + C\omega^4. \qquad (1)$$

The resulting function is integrated with respect to ω to obtain the spin I, namely,

$$I_\gamma(\omega) - I_{\gamma 0} = A\omega + (B/3)\omega^3 + (C/5)\omega^5 + 1/2. \qquad (2)$$

The basic assumption of the technique is that of no alignment at rotational frequency $\omega \sim 0$, i.e., $I_{\gamma 0} = 0$. This is indeed in perfect agreement with our HBF calculations, as discussed below in Sec. IV. The dynamic moment of inertia is displayed in Fig. 6(b). Let us first make a comment on the procedure used to calculate the moment of inertia. Although the band is characterized by a sequence of $\Delta I = 1\hbar$ transitions, this band is divided for convenience into two $\Delta I = 2\hbar$ branches when calculating the moment of inertia. Looking at the moment of inertia, one notes the presence of a shallow minimum at a rotational frequency of $\hbar\omega \sim 0.19$ MeV, a feature that will be commented upon later. Obviously, the two points in the vicinity of this minimum, which strongly deviate from the otherwise smooth pattern, should be excluded from the Harris fit. The low statistics in the γ-ray spectra measurements (see Fig. 5) leads to uncertainties in the determination of the parameters entering the fitted expression [Eq. (2)]. The best fit leads to the estimate $I_0 = 8.1 \pm 1.9\hbar$ for the bandhead level. In addition, the spin-fitting method introduced by Wu *et al.* [41] has been used as a cross-check of the above spin determination. The method gives for integer I_0 a minimum in the χ^2 function at $I_0 = 8\hbar$. Finally, both methods are fully consistent with spin $I_0 = 8\hbar$ for the bandhead.

D. Structure assignment

In the $N = 150$ (^{246}Cm and ^{248}Cf) isotones the presence of the 8^- isomeric states is a common feature of this region, as was already pointed out in the introduction. The neutron $7/2^+[624]_\nu \otimes 9/2^-[734]_\nu$ nature of this state has then been firmly established on the basis of different experimental means, e.g., transfer reactions and β decay. The similarity of the level schemes between ^{252}No and those for the other isotones makes the assumption that also in this case the decay proceeds through the two-neutron components of the wave functions. A direct measurement of the structure of the isomeric states found in ^{252}No produced via the fusion-evaporation reaction can be performed via the study of the γ rays emitted during the de-excitation of the band built on the isomeric state. The electromagnetic properties of the states were deduced and the magnetic moment, or the g_K gyromagnetic factor, was inferred. The g_K factor depends on the two-quasiparticle configuration and depends in general on the scenario. It is therefore a crucial quantity for understanding the isomer structure and for a comparison with the models. As mentioned in the introduction, the $K^\pi = 8^-$ isomeric state can be interpreted either as a two-quasiproton $(9/2^+[624]_\pi \otimes 7/2^-[514]_\pi)$ or two-quasineutron $(7/2^+[624]_\nu \otimes 9/2^-[734]_\nu)$ configuration. Although new HFB calculations are presented in this article, the complex formalism for calculating rigorously the magnetic moment has not yet been implemented in the HFB code. Therefore the gyromagnetic factor inferred from Woods-Saxon-based calculations will be used. According to [42], the g_K factor for these two 8^- configurations are 0.01 $(7/2^+[624]_\nu \otimes 9/2^-[734]_\nu)$ and 1.01 $(9/2^+[624]_\pi \otimes 7/2^-[514]_\pi)$, respectively. It is interesting to note that these values are very close to the asymptotic limit for singlet states ($\Sigma = 0$) which are energetically favored according to the Gallagher rule [43]. In this case the gyromagnetic factor of the spin cancels and one has only a contribution from the angular momentum I of the two protons ($g_K = g_l^p = 1$) or neutrons ($g_K = g_l^n = 0$). To determine the experimental g_K factor, the well-known relationship between the observed

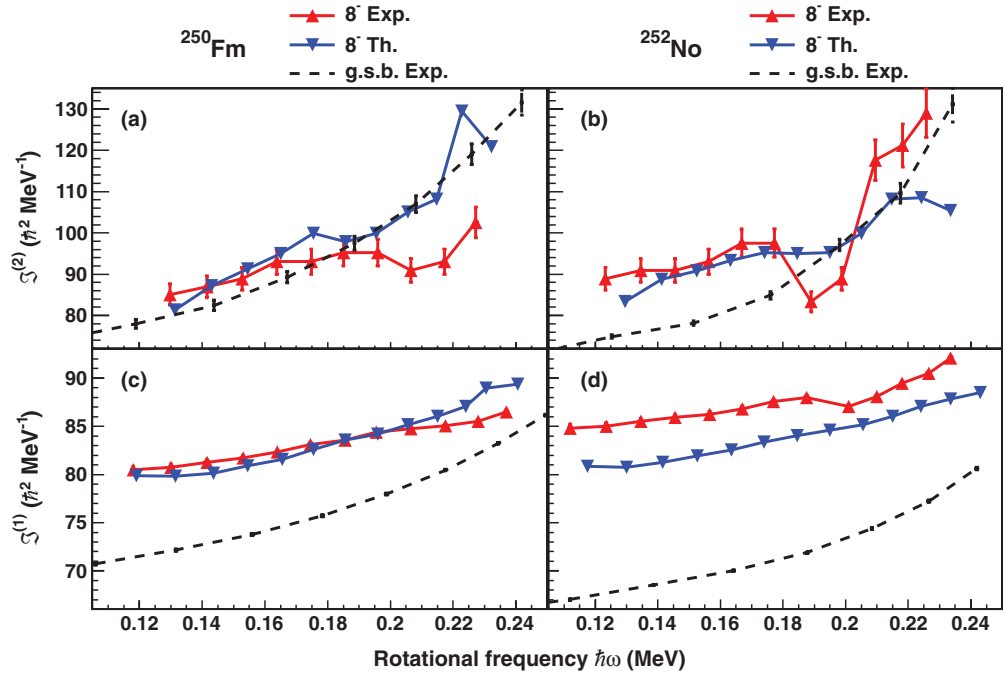

FIG. 6. (Color online) (a) and (b) Dynamic moment of inertia $\mathcal{J}^{(2)}$ vs $\hbar\omega$ for the ground-state rotational band (dashed black lines) and for the isomeric $K^\pi = 8^-$ band, for the ^{250}Fm and ^{252}No (red triangles) isotones. (c) and (d) Same as (a) and (b) but for the kinematic moments of inertia. Triangular blue marks represent theoretical calculations using the D1S Gogny force. See text for details.

γ-ray branching ratio, the g_K factor, and decay probabilities was used, i.e.,

$$R^{the} = \frac{I(M1; J \to J-1)}{I(E2; J \to J-2)} = \frac{1.76[E_\gamma(M1)]^3 B(M1)\ \mathrm{s}^{-1}}{1.22[E_\gamma(E2)]^5 B(E2)\ \mathrm{s}^{-1}}, \quad (3)$$

where the reduced transition probabilities $B(E2)$ and $B(M1)$ are

$$B(E2, J \to J-2) = \frac{5}{16\pi} e^2 Q_0^2 \langle JK20|(J-2)K\rangle^2 \quad (4)$$

and

$$B(M1, J \to J-1) = \frac{3}{4\pi}\left(\frac{e\hbar}{2Mc}\right)^2 (g_K - g_R)^2 K^2 \langle JK10|(J-1)K\rangle^2. \quad (5)$$

The core gyromagnetic factor is taken to be $g_R = Z/A = 0.4$ in the hydrodynamic limit. While the g_K factor changes strongly from one configuration to another, the electric quadrupole moment Q_o does not exhibit large differences and is accurately predicted by the models. We have here taken that for the neutron two-quasiparticle HFB value, namely, $Q_o = 13.75\ e$ b. The experimental branching ratios are given in Table I for the three initial states for which both interband $M1$ and intraband $E2$ transitions were measured. We have assumed a small mixing ratio for the $\Delta I = 1\hbar$ transition according to [44]. Unfortunately, the γ-ray transitions are observed with low intensity, which translates into large error bars for the experimental ratio. According to Eq. (3), the branching ratio is a parabolic function of g_K, as shown in Fig. 7 in the case of the $I^\pi = 14^-$ initial level. Decay probabilities lie on this parabola: $7/2^+[624]_\nu \otimes 9/2^-[734]_\nu$ with $g_K = 0.01$ (square symbol) and $9/2^+[624]_\pi \otimes 7/2^-[514]_\pi$) with $g_K = 1.01$ (circle symbol). The experimental intensity ratio is shown with the yellow area. The intersection of the experimental intensity ratio value with the parabola gives two possible g_K values. It is clear that only the $K^\pi = 8^-$ neutron configuration agrees well with the measured ratio. The same conclusion can be drawn for the 15^- and 16^- initial states.

However, using single intensity ratios from low-statistic spectra can lead to large uncertainties. It is therefore more appropriate in this case to apply the analytical method described in detail in [45]. The technique is based on the idea that the transitions in a strongly coupled band will have easily visible stretched $E2$ transitions and interband $\Delta I = 1\hbar$ transitions clustered at low energies. As the band is built on a particular configuration the branching ratios in the band are easily modeled by using this configuration as input. This gives an estimate of the number of counts one would expect to find in this $\Delta I = 1\hbar$ region in the spectrum, even if the statistics are not large enough to analyze individual peaks. An "integral branching ratio" is therefore extracted, and this may often take

TABLE I. Experimental intensity ratios $I(M1)/I(E2)$.

Initial level	$I(M1)/I(E2)$	R_{exp}
16^-	$I_\gamma(182)/I_\gamma(354)$	0.49 ± 0.41
15^-	$I_\gamma(172)/I_\gamma(334)$	0.37 ± 0.37
14^-	$I_\gamma(162)/I_\gamma(313)$	0.65 ± 0.37

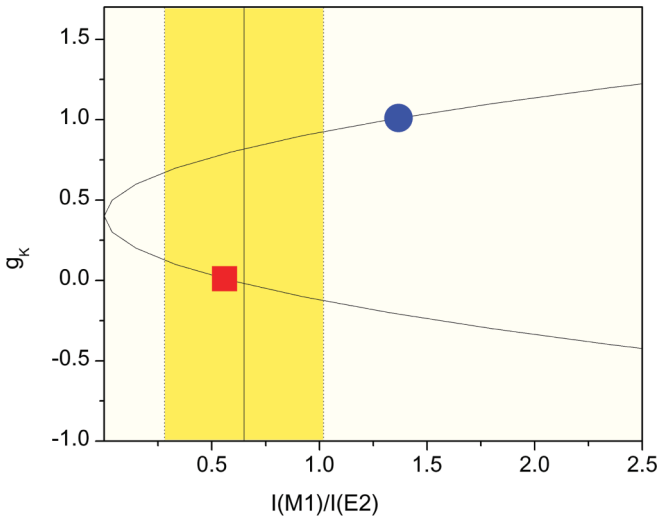

FIG. 7. (Color online) The relationship between intensity ratio $I(M1)/I(E2)$ and g_K, showing the values for the expected neutron (red square) and proton (blue circle) configurations compared with the experimental ratio (yellow area) for the decay of the $I^\pi = 14^-$ level. See text for details.

the form of an upper limit to compare the experimental spectral shape to that predicted by the rotational model based on the different possible configurations. The details are explained in [45].

The number of experimentally deduced counts is denoted with N_0 and the number of expected counts in the same region for both candidate configurations with N_n (two-quasineutron state $7/2^+[624]_\nu \otimes 9/2^-[734]_\nu$) or N_p (two-quasiproton state $9/2^+[624]_\pi \otimes 7/2^-[514]_\pi$), using the easily observed intensity of the $E2$ transitions as normalization. This method was applied for the intraband transitions $I^\pi = 14^-$ to $I^\pi = 19^-$. The comparison between the deduced values N_0 and the Gaussian probability distribution found for the two different scenarii shown in Fig. 8 favors the neutron structure being about 3 times as probable as the proton structure (56% versus 14%) [45].

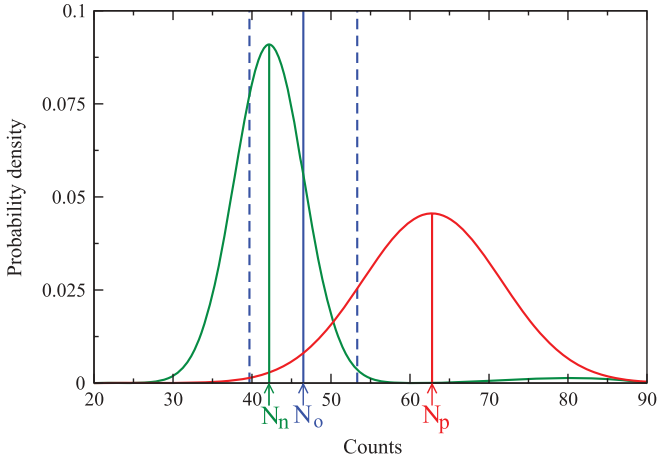

FIG. 8. (Color online) Expected total counts N_n for the two-quasiparticle neutron configuration (green) and N_p for the two-quasiparticle proton configuration (red) and observed counts N_o (blue line) along with attached uncertainties (dashed blue lines).

This technique was also applied to the rotational band built on top of the $K^\pi = 8^-$ isomer in ^{250}Fm [45], the result being fully consistent with the interpretation of Greenlees *et al.* [20].

This method combined with the measurement of the $M1/E2$ ratio provides a strong experimental indication of the isomeric structure as a spin singlet two-quasineutron state. With $K^\pi = 8^-$ as the bandhead, the likely configuration is $7/2^+[624]_\nu \otimes 9/2^-[734]_\nu$.

E. Hindrance factor

Long-lived K isomers occur because the decay via transitions with a large ΔK is strongly hindered: there is no state with similar wave function available for the decay. These states with a high degree of K purity can only be obtained for axially symmetric nuclei. The reduced hindrance factor f_ν gives an indication on the "goodness" of the quantum number K, or the K purity of the state. It is defined as

$$f_\nu = \left(T^\gamma_{1/2}/T^W_{1/2}\right)^{1/\nu}, \tag{6}$$

where $T^\gamma_{1/2}$ is the partial γ-ray half-life and $T^W_{1/2}$ is the Weisskopf single-particle estimate. The exponent $1/\nu = 1/(\Delta K - \lambda)$ represents the degree of forbiddenness with λ being the multipolarity of the decay radiation. A value of $f_\nu \sim 100$ is expected according to the systematics of Löbner [46]. In ^{252}No, the reduced hindrance factor can be obtained from the decay to the $K^\pi = 0^+$ ground-state band ($8^- \to 8^+$ $E1$ transition at 710 keV) or from the decay to the $K^\pi = 2^-$ octupole band ($8^- \to 7^-$ $M1$ transition at 25 keV). Using a branching ratio of 4% for the $E1$ transition at 710 keV [15], one obtains f_ν ($E1$, $8^- \to 8^+$) = 178 and f_ν ($M1$, $8^- \to 7^-$) = 218. The high value of the reduced hindrance factor testifies to the high purity of the two-quasiparticle $K^\pi = 8^-$ isomer and the small degree of mixing with both the ground-state band and the $K^\pi = 2^-$ excited band. This value favorably compares with the $K^\pi = 8^-$ isomer in the $N = 150$ isotones: f_ν (^{250}Fm, $E1$, $8^- \to 8^+$) = 213, f_ν (^{250}Fm, $M1$, $8^- \to 7^-$) = 192 [20], f_ν (^{246}Cm, $E1$, $8^- \to 8^+$) = 212 [47], and f_ν (^{244}Pu, $E1$, $8^- \to 8^+$) ~200 [17].

III. THEORETICAL FRAMEWORK

Mean-field calculations were performed in triaxial oscillator bases including 14 shells using the D1S Gogny force [21,22]. The neutron and proton single-particle states obtained at equilibrium deformation are shown in Fig. 9, where single neutron gaps are predicted at $N = 150$ and $N = 152$ while the proton main gaps are predicted to be at $Z = 98$ and 104. The deformed shell gaps indicated by the experiments are $N = 152$ and $Z = 100$ [1]. The present neutron and proton level schemes at equilibrium deformation differ from those in previous publications [9,16,48,49].

To establish our notation we first define the quasiparticle vacuum HFB energy from minimization of the functional

$$\delta \langle \Phi | \widehat{H} - \lambda_Z \widehat{Z} - \lambda_N \widehat{N} | \Phi \rangle = 0, \tag{7}$$

where $\widehat{H}$ is the nuclear Hamiltonian, and

$$\langle \Phi | \widehat{N} | \Phi \rangle = N; \ \langle \Phi | \widehat{Z} | \Phi \rangle = Z, \tag{8}$$

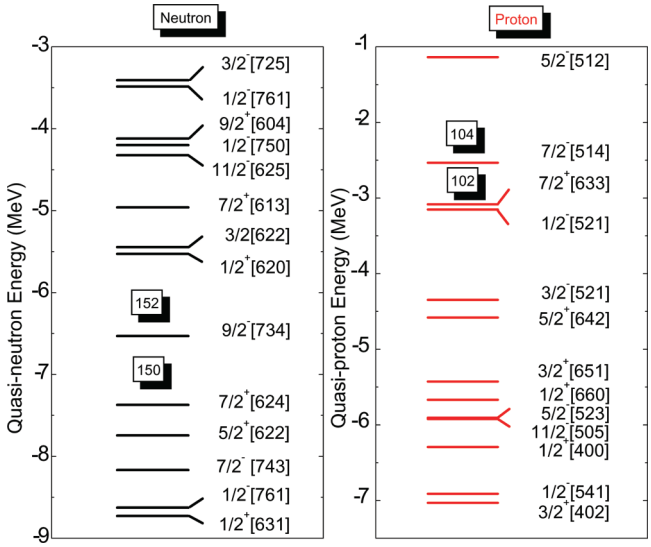

FIG. 9. (Color online) Single-particle energies for neutron and proton states in ^{252}No at axial equilibrium deformation of the HFB energy, where the charge quadrupole moment is $Q_0 = 13.75\,e$ b. The labels $[Nn_z\Lambda]$ are assigned by analogy with a Nilsson diagram.

with $\widehat{Z}$ and $\widehat{N}$ as the proton and neutron number operators, respectively, and λ_Z and λ_N Lagrange multipliers.

The two-quasiparticle excitations are sought for using blocking calculations also performed in the same HFB framework. Here, a trial state $|\Phi'_{ij}\rangle = \eta_i^+ \eta_j^+ |\Phi_{ij}\rangle$ is defined, in which η_i^+ is a quasiparticle creation operator. The index i (respectively j) refers to the set of quantum numbers of a one-quasiparticle orbital labeled i (respectively j) and located in the vicinity of the Fermi energy of the unblocked HFB solution $|\Phi\rangle$. Then the equation

$$\delta\langle\Phi'_{ij}|\widehat{H} - \lambda_N\,\widehat{N} - \lambda_Z\,\widehat{Z}|\Phi'_{ij}\rangle = 0 \qquad (9)$$

is solved, and the two-quasiparticle excitation energy is obtained as the difference [22]:

$$E^{ij}_{2qp} = \langle\Phi'_{ij}|\,\widehat{H}\,|\Phi'_{ij}\rangle - \langle\Phi|\,\widehat{H}\,|\Phi\rangle. \qquad (10)$$

If time-reversal symmetry is assumed, the signature partner pairs with angular momentum projections on the z axis, $K_- = K_1 - K_2$ and $K_+ = K_1 + K_2$, and parity $\pi = \pi_1 \cdot \pi_2$ are degenerate in energy.

The wave functions in the rotating frame actually are subject to fulfilment of spacial symmetries, namely, (i) parity operator $\widehat{\Pi}$, (ii) z signature $\hat{S}_z = i\hat{R}_3\ (\pi)$ with $\hat{R}_3$ as the operator for rotation around the z axis, and (iii) the product $\hat{K}\cdot\widehat{\Pi_2}$ of operators, where $\hat{K}$ stands for time-reversal symmetry and $\widehat{\Pi_2}$ for reflectiion with respect to the x-z plane. These symmetries form a set of self-consistent symmetries which are commuting only for the vacuum HFB solutions of a system rotating around the z axis [50]. Furthermore, two-quasiparticle excitations rotating along the x axis do break the signature symmetry here taken along the z axis and defined as

$$\hat{S}_z = ie^{-i\pi\hat{J}_z}, \qquad (11)$$

where $\hat{J}_z$ is the projection of angular momentum onto the z axis. The z-signature is broken because $\hat{J}_x$, the projection of angular momentum onto the x-axis, and $\hat{S}_z$ do not commute [51].

Within the HFB theory expressed in the rotating frame, the aligned two-quasiparticle internal structure of a nucleus with total angular momentum I, neutron number N, and proton number Z is determined by solving the equation for the dynamical quasiparticle vacuum $|\Phi'^{\omega}_{ij,+}\rangle$:

$$\delta\left\langle\Phi'^{\omega}_{ij,+}\right|\ \widehat{H} - \omega\,\widehat{J}_x - \lambda_N\,\widehat{N} - \lambda_Z\,\widehat{Z}\ \left|\Phi'^{\omega}_{ij,+}\right\rangle = 0, \quad (12)$$

with the dynamical constraint on the x component J_x of the total angular momentum I defined by

$$J_x = \left\langle\Phi'^{\omega}_{ij,+}\right|\hat{J}_x\left|\Phi'^{\omega}_{ij,+}\right\rangle = \sqrt{I\,(I+1) - \langle J_z\rangle^2}, \qquad (13)$$

where the indexes ij stand for the blocked orbitals and the plus sign indicates aligned configurations.

In ^{250}Fm and ^{252}No, the two-quasiparticle signature partner bandheads with $\langle J_z\rangle^{\pi} = K^{\pi}_{+} = 8^-$ and $\langle J_z\rangle^{\pi} = K^{\pi}_{-} = 1^-$ quantum numbers are built from the neutron $9/2^-$ and $7/2^+$ levels closest to the Fermi energies (see Fig. 9). For both nuclei, breaking time-reversal symmetry removes the energy degeneracy of the signature partner $K^{\pi}_{-} = 1^-$ and $K^{\pi}_{+} = 8^-$ head levels. The two head levels display intrinsic excitation energies which differ by 200 keV. The aligned $K^{\pi} = 8^-$ two-quasiparticle head levels are lowest in energy. Excitation energies of the $K^{\pi}_{-} = 1^-$ and $K^{\pi}_{+} = 8^-$ solutions are as follows: $E_x(K^{\pi}_{-} = 1^-) = 1.138$ MeV, $E_x(K^{\pi}_{+} = 8^-) = 0.920$ MeV and $E_x(K^{\pi}_{-} = 1^-) = 1.195$ MeV, $E_x(K^{\pi}_{+} = 8^-) = 0.982$ MeV, for ^{250}Fm and ^{252}No, respectively. The arithmetic mean energies of these signature-partner pairs are $E_{m,2qp} = 1.029$ MeV and $E_{m,2qp} = 1.031$ MeV for ^{250}Fm and ^{252}No, respectively. Both mean energies are close to those obtained previously in blocking calculations without breaking time-reversal symmetry, namely, 1.010 MeV (^{250}Fm) and 1.070 MeV (^{252}No) [22]. These results are in qualitative agreement with expectations based on the Gallagher rule [43]. After correcting for zero-point energy $E_0 = 8\hbar^2/2\mathcal{J}^{(1)}$, that is, $E_0 = 49$ keV (51 keV) for ^{252}No (^{250}Fm) as inferred from the kinematic moments of inertia $\mathcal{J}^{(1)}$ shown in Fig. 9, the calculated $I^{\pi} = 8^-$ head level energies are $E_x(I^{\pi} = 8^-) = 0.971$ MeV and $E_x(I^{\pi} = 8^-) = 1.031$ MeV for ^{250}Fm and ^{252}No, respectively. These calculated excitation energies are reasonably close to those found in experiments, namely, $E_x = 1.199$ MeV and $E_x = 1.254$ MeV for ^{250}Fm and ^{252}No, respectively.

IV. MOMENT OF INERTIA

A. General trend

The moments of inertia provide a tool to quantify the robustness and rigidity of the K isomer and the rotational band. The experimental kinematic and dynamic moments of inertia $\mathcal{J}^{(1)}$ and $\mathcal{J}^{(2)}$, respectively, are shown in Fig. 6 for the ground-state band (dashed black lines) and the $K^{\pi} = 8^-$ bands in the ^{250}Fm and ^{252}No (red triangles) isotones. Blue triangles represent theoretical results using the D1S Gogny force. Excellent agreement has been found for the ground-state bands [22] using the same theoretical framework. It is worth

noting that a good degree of accuracy is also obtained for the $K^\pi = 8^-$ two-quasiparticle isomeric band as far as the moment of inertia and the excitation energies are concerned. The agreement is in particular very good at low frequency, especially for ^{250}Fm. One should again note some irregularities in the moment of inertia that will be discussed in Sec. IV B.

In general, the moment of inertia of the ground-state band increases with increasing frequency under the influence of the Coriolis antipairing force, which slowly aligns the angular momentum along the rotation axis. On the other hand, the two-quasiparticle configuration of the excited band blocks the neutron pairing, increasing the kinematic moment of inertia already at low frequencies. At $\hbar\omega \sim 0.12$ MeV, the gain is $\sim$10% for ^{250}Fm and reaches $\sim$30% for ^{252}No. This effect is well known in odd-mass nuclei compared to their even-even neighbors. More generally, the moment of inertia is expected to increase with the number of quasiparticles involved. It is important to stress that the difference in the moment of inertia between the ground-state and the $K^\pi = 8^-$ bands reflects a change in pairing energy, not in deformation. Indeed, the neutron pairing energy has been found null in the present blocking HFB calculations while a quadrupole moment of 13.75 e b is predicted for the ground state close to 13.84 e b for the $K^\pi = 8^-$ isomeric state. In ^{250}Fm, the values are 13.39 e b (ground state) and 13.47 e b ($K^\pi = 8^-$).

In the $K^\pi = 8^-$ bands, the rotor is not only more rigid but also more stable with the rotation than the ground-state band. This can be inferred from the comparison of $\mathcal{J}^{(1)}$ and $\mathcal{J}^{(2)}$. Indeed, (i) the kinematic moment of inertia is almost constant as a function of the rotational frequency, and (ii) the difference between $\mathcal{J}^{(1)}$ and $\mathcal{J}^{(2)}$ is small (at least at low rotational frequency). In other words, there is little contribution from the unpaired nucleons as soon as the nucleus rotates. The alignment of the angular momentum along the rotation axis is small because of the robustness of the high-K configuration.

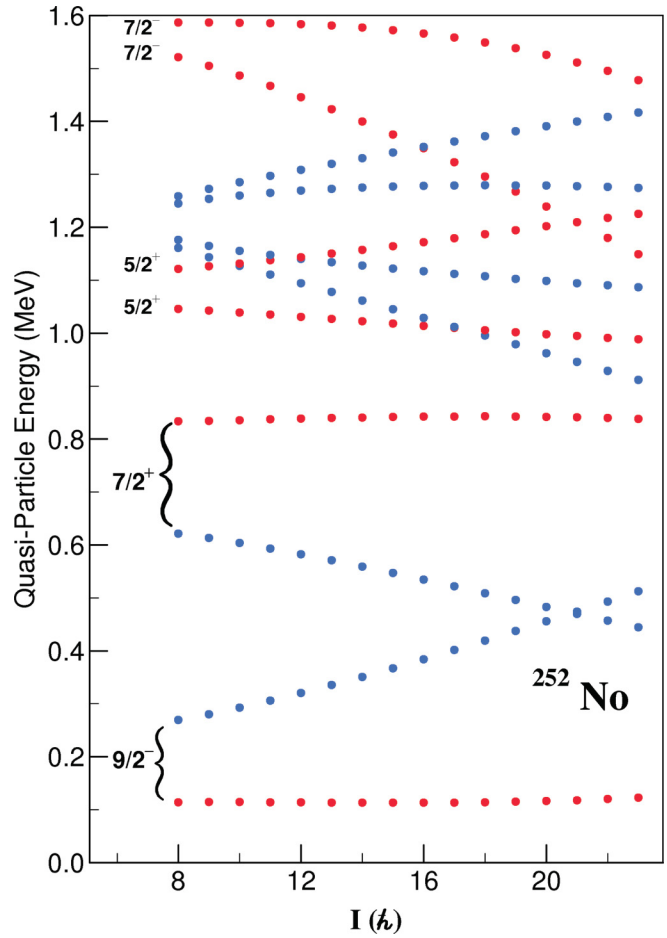

FIG. 10. (Color online) Quasiparticle energies calculated vs spin I for neutrons. The color code is for the occupation probabilities. Occupied orbitals are shown in red and empty ones in blue. States are labeled with quantum numbers π (parity) and Ω (projection onto the x axis of quasiparticle angular momentum).

B. Anomaly in the moment of inertia

As mentioned above, the regularity of rotational bands changes at $\hbar\omega \sim 0.19$ MeV for ^{252}No but also for ^{250}Fm at a slightly higher frequency: the moment of inertia decreases and seems to recover its initial trend at higher frequency. The theoretical moments of inertia also display irregularities but they are less pronounced.

Irregularities in the moment of inertia often result from the crossing of bands having the same spin and parity. When the bands get closer in energy, they repel mutually, inducing some perturbations of the level energies, displacements that are magnified in the dynamic moment of inertia. One of the bands displays a bump in the moment of inertia while the interacting partner displays a dip. As another consequence of the adiabatic interaction, the two bands exchange their single-particle configuration along the crossing. In a more general context, the time-dependent interaction of quantum systems is known as a Landau-Zener crossing [52]. Many examples of band crossings are found along the nuclear chart, for instance in superdeformed bands [53].

1. Theoretical analysis

To test the hypothesis of band crossing the investigation of Routhian properties has been carried out. The neutron quasiparticle energies in the rotating frame (Routhians) are shown in Fig. 10. They are labeled with quantum number π (parity) and Ω (projection onto the x axis of quasiparticle angular momentum at $I = 8\hbar$). Let us first note that the occupied quasiparticle orbitals labeled with the quantum numbers $\Omega^\pi = 9/2^-, 7/2^+$ display energies that are almost constant as a function of spin at least up to spin $I = 25\hbar$. This is consistent with the robustness of the $K^\pi = 8^-$ quasiparticle configuration as a function of the rotation. Also, these calculations did not show any orbital crossing among occupied orbitals with $\pi = -$.

The irregularities in the calculated moments of inertia should be correlated to the evolution of another parameter. Inspection of the proton pairing energy as a function of spin (see Fig. 11) does not reveal any changes or a pairing collapse that could induce the anomalies in the theoretical moments of inertia.

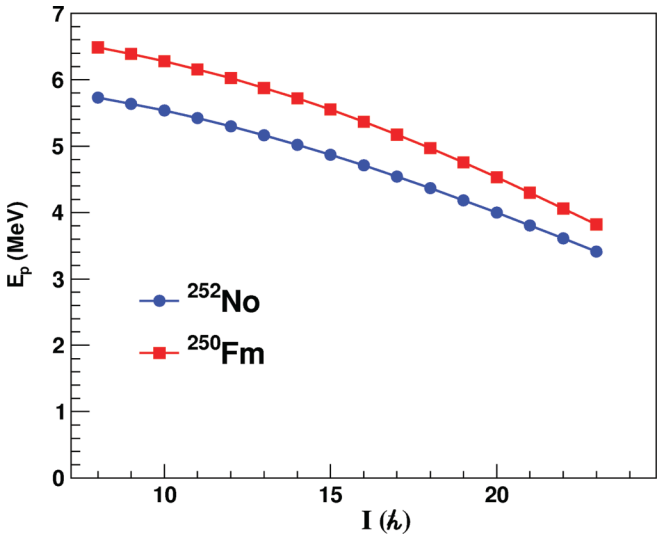

FIG. 11. (Color online) Proton pairing energy for ^{250}Fm and ^{252}No.

As customary in nuclear structure calculations, the axial and triaxial quadrupole deformations β and γ are defined as functions of the mass quadrupole moments Q_{20} and Q_{22}, respectively, as

$$\beta = \sqrt{\frac{\pi}{5}}\frac{\sqrt{Q_{20}^2 + 3Q_{22}^2}}{A\langle r^2\rangle} \tag{14}$$

and

$$\gamma = \arctan\sqrt{3}\frac{Q_{22}}{Q_{20}}, \tag{15}$$

where A and $\langle r^2\rangle$ are the nuclear mass numbers and mean square radius of the mass distribution, respectively, and where

$$\langle r^2\rangle = \tfrac{3}{5}(r_0 A^{1/3})^2 \tag{16}$$

with $r_0 = 1.2$ fm. The deformation parameters have here been calculated using the above equations for Q_{20} and Q_{22} values calculated for each spin value from $I = 8\hbar$ to $I = 24\hbar$. Over this spin sequence β and γ values remain constant to less than 3% and 1%, respectively, for ^{252}No and ^{250}Fm. These features suggest no shape evolution through the bands, which may explain the irregular pattern displayed by the calculated dynamic moments of inertia (see Fig. 6).

2. *Experimental band crossing*

We next investigate whether the irregularities observed in the $\mathcal{J}^{(2)}$ measurements stem from band crossing. One of the possible candidates to cross the $K^\pi = 8^-$ band at $\hbar\omega \sim 0.19$ MeV is the side band $K^\pi = 2^-$. It is not excluded that the $K^\pi = 8^-$ band could instead cross an unobserved band such as $K^\pi = 7^-$ predicted by Delaroche *et al.* [22] and observed in the isotone ^{248}Cf [54] at 1.5 MeV. Returning to the first hypothesis for which we have experimental information, we see that both bands have the same $\pi = -$ parity and similar bandhead excitation energies (see Fig. 4). To illustrate such a scenario we have plotted in Fig. 12 experimental excitation energies as a function of spin for the ground-state band (black

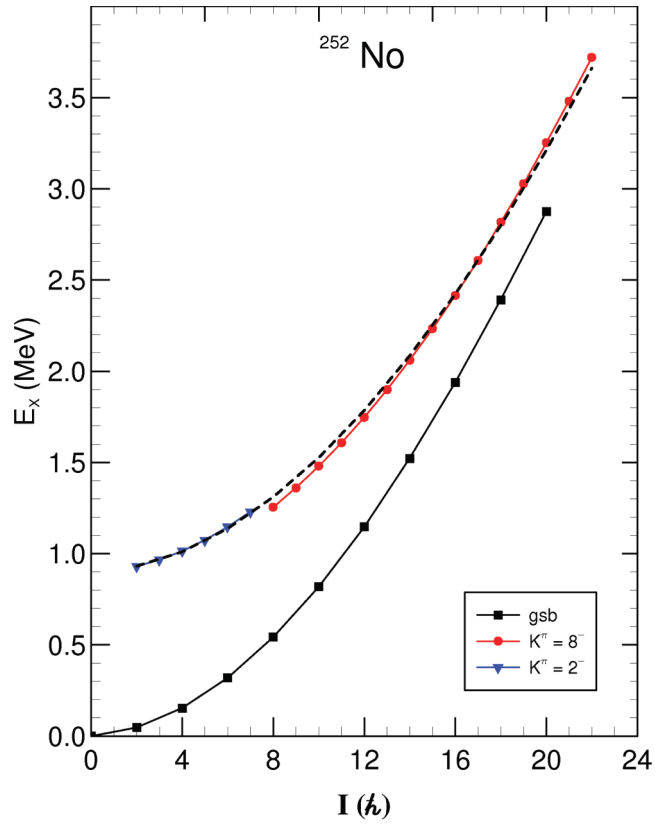

FIG. 12. (Color online) Energy vs spin for the ground-state rotational band (black dots), $K^\pi = 2^-$ excited band (blue triangles), and isomeric rotational band (red dots) for ^{252}No. The dashed line is for an extrapolation of the observed $K^\pi = 2^-$ band to spins higher than $I = 7\hbar$.

squares), the $K^\pi = 8^-$ band (red dots), the $K^\pi = 2^-$ band (blue triangles), as well as a smooth extrapolation of this latter band to spins higher than $I = 8\hbar$ (dashed line). As can be seen, the dashed curve crosses the red curve in the vicinity of the spin value $I = 17\hbar$, which is close to the rotational frequency $\hbar\omega \sim 0.19$ MeV where the shallow minima in the $\mathcal{J}^{(2)}$ values is observed. Due to the lack of statistics and to hindered feeding, the higher frequency portion of the $K^\pi = 2^-$ band is not observed. It is therefore impossible to check whether this band would display a bump in $\mathcal{J}^{(2)}$ values at approximately the same frequency where $\mathcal{J}^{(2)}$ values of the $K^\pi = 8^-$ band are showing a bump. One should remember also that the $K^\pi = 2^-$ band is observed at low spin because it is fed by a decay-out branch of the $K^\pi = 8^-$ level. If the assumption of band crossing holds correct, the observed $K^\pi = 8^-$ band crosses the $K^\pi = 2^-$ band at $\hbar\omega \sim 0.19$ MeV, and the band configurations will get exchanged: the $K^\pi = 2^-$ configuration becomes energetically favored and preferentially fed at higher frequencies. Such an interpretation holds too for the excited bands in ^{250}Fm where the crossing takes place at slightly different spin and frequency, namely, $I \sim 16\hbar$ and $\hbar\omega \sim 0.21$ MeV. Although K is no longer a good quantum number at higher spins, our scenario would require almost degenerate unperturbed states. Hence the suggested scenario will remain tentative until new data collected in higher statistic measurements are available.

3. Discussion

The presence of side bands with spin and parity 2^- seems to be a common feature in $N = 150$ isotones (e.g., ^{252}No, ^{250}Fm [20], ^{248}Cf [19], and ^{246}Cm [16,18]). The similar and low excitation energy ($E_x \sim 1$ MeV) of the $K^\pi = 2^-$ bandhead level suggests a collective character (namely, octupole correlations). On the theoretical side, structure models are predicting $\pi = -$ levels at low excitation energy for this mass region [24,55]. Within the RPA the low-energy $K^\pi = 2^-$ level is calculated for ^{252}No at $E_x = 0.998$ MeV [24], close to the experimental value. This study did not provide the major components of the $K^\pi = 2^-$ state wave function. Such structure information is available for ^{246}Cm, another $N = 150$ isotone, for which the two-neutron $9/2^-[734]_\nu \otimes 5/2^+[622]_\nu$ and two-proton $3/2^-[521]_\pi \otimes 7/2^+[633]_\pi$ quasiparticle excitations form the dominant components of the lowest $K^\pi = 2^-$ state [55]. More recently, projected shell-model calculations performed for $N = 150$ isotones (including ^{252}No) have focused on nonaxial octupole correlations [56]. It is interesting to note that the excitation energy range $E_x \sim 2.7$–3.2 MeV for states with spins from $I^\pi = 16^-$ to $I^\pi = 18^-$ in the calculated $K^\pi = 2^-$ band of ^{252}No is in qualitative agreement with the energy $E_x \sim 2.7$ MeV where crossing between the $K^\pi = 2^-$ and $K^\pi = 8^-$ bands is expected to occur (see Fig. 12).

Obviously, the next generation of HFB calculation in the rotating frame would consist in breaking time-reversal symmetry, z-signature, as well as left-right symmetry. This task is beyond the scope of the present work.

If the interpretation as an octupole character for the $K^\pi = 2^-$ band and interpretation of the band crossing are correct, it would induce an interesting feature at high angular momentum. The $K^\pi = 0^-$ octupole vibration predicted close to the $K^\pi = 2^-$ component [24] contains only the $\alpha = 1$ signature sequence. The Coriolis mixing between $\alpha = 1$ states in $K^\pi = 0^-$ and $K^\pi = 2^-$ bands induces an odd-even signature splitting (see, for instance, [57]). As discussed previously the top of the $K^\pi = 8^-$ isomeric band should mutate to a $K^\pi = 2^-$ character with therefore an odd-even signature splitting feature. Evidence for such a staggering has been found in both ^{250}Fm and ^{252}No but the statistical uncertainties are too large to draw any conclusions. More statistics and/or extension of measurements to higher spins would clarify this assumption and more generally the anomalies in the moments of inertia.

V. SUMMARY AND CONCLUSION

In this paper we reported on a detailed investigation of nonyrast states in ^{252}No. In-beam γ-ray spectroscopy was performed at the University of Jyväskylä using the recoil-decay tagging technique, with an emphasis on collective states built on the two-quasiparticle $K^\pi = 8^-$ isomer. The study of this rotational band and decay toward the ground state provides valuable information on the single-particle structure, collectivity, and K isomerism. The large reduced hindrance factor and the strong stability of the rotational band support high purity of the K isomeric state, which persists with increasing rotational frequency. The single-particle configuration component in the $K^\pi = 8^-$ level is probed by the interband $M1$ and intraband $E2$ experimental γ-ray intensity ratios that provide an indirect measurement of the g_K gyromagnetic factor. As deduced from the data a two-quasiparticle neutron state $7/2^+[624]_\nu \otimes 9/2^-[734]_\nu$ is suggested for the $K^\pi = 8^-$ band. The $K^\pi = 8^-$ isomers in other $N = 150$ isotones with lower masses, i.e., ^{246}Cm, ^{248}Cf, and ^{250}Fm, are thought to be built on the same two-neutron configuration.

The $\mathcal{J}^{(2)}$ values inferred from γ-ray measurements for the ^{252}No and ^{250}Fm $K^\pi = 8^-$ bands were compared with HFB calculations in the rotating frame that break time-reversal and z-signature self-consistent symmetries. A good overall agreement between measurements and calculations is obtained for bandhead energies and moments of inertia. However, the calculations failed in reproducing $\mathcal{J}^{(2)}$ values which display a shallow minimum observed at frequency $\hbar\omega \sim 0.18$–0.22 MeV for ^{252}No. This feature is tentatively interpreted as a crossing between the $K^\pi = 8^-$ and $K^\pi = 2^-$ bands, the latter band not being observed for spins beyond $I = 7\hbar$. We do not exclude the possibility that the $K^\pi = 8^-$ band might instead cross another unobserved band. Measurements with higher statistics would be a valuable asset to clarify the issue. The systematic occurrence of low-energy $K^\pi = 2^-$ excitations in $N = 150$ isotones is strongly suggestive of octupole correlations. Such correlations are ignored in the present microscopic model. However, they could be handled by breaking one more self-consistent symmetry, namely, the left-right symmetry. The hope is that extended cranking HFB calculations would (i) shed light on the interpretation of irregularity observed in the $\mathcal{J}^{(2)}$ moment of inertia of the $K^\pi = 8^-$ band at frequency $\hbar \approx 0.18$–0.22 MeV and (ii) provide a guide to infer quantum numbers of the quasiparticle components of the $\pi = -$ crossing band. Such calculations are under consideration. It would also be a valuable task to challenge predictions based on quasiparticle random phase approximation (QRPA) calculations [58], provided that the theory is extended to the rotating frame. Such an approach proved successful previously for the interpretation of back-bending phenomena observed in $\pi = -$ superdeformed bands of Hg isotopes [59,60]. Running QRPA calculations in the rotating frame with the D1S force as sole input would be a formidable task that most likely is manageable with the availability of algorithms and computers of the next generation.

Finally, it would be interesting to extend the present measurement of $K^\pi = 8^-$ band at high spin in other $N = 150$ isotones, e.g., ^{246}Cm and ^{248}Cf, and obviously in the heavier ^{254}Rf nuclide. Extension of the $K^\pi = 8^-$ rotational bands in ^{250}Fm and ^{252}No to spins higher than $I^\pi = 22^-$ would also help to clarify the anomalies in the moment of inertia.

ACKNOWLEDGMENTS

We thank the accelerator staff at the University of Jyväkylä for the excellent performance of the ion source and accelerator. H. Goutte is acknowledged for involvement in developing the cranking HFB code. This work has been supported by the EU-FP6-I3 Project EURONS No. 506065, the Academy of Finland [CoE Nuclear and Accelerator Based Physics Programme at JYFL, grants to PTG (111965) and CS (209430)], the EC "Marie Curie Actions grant," the UK STFC, and the US

Department of Energy (Contract No. DE- AC02-06CH11357). MV appreciates support from the Slovak grant agency VEGA (Contract No. 2/0105/11). SA was supported by the Slovak Research and Development Agency Contract No. APVV-0105-10 and VEGA Contract No. 1/0613/11. We thank the UK-France (STFC/IN2P3) Loanpool and the GAMMAPOOL European Spectroscopy Resource for the loan of detectors for JUROGAM. This work has benefited from the use of TNT2 cards, developed and financed by CNRS/IN2P3 for the GABRIELA project.

[1] R.-D. Herzberg and P. T. Greenlees, Prog. Part. Nucl. Phys. **61**, 674 (2008).
[2] F. R. Xu, E. G. Zhao, R. Wyss, and P. M. Walker, Phys. Rev. Lett. **92**, 252501 (2004).
[3] S. Hofmann *et al.*, Eur. Phys. J. A **10**, 5 (2001).
[4] F. P. Heßberger *et al.*, Eur. Phys. J. A **43**, 55 (2010).
[5] D. Peterson *et al.*, Phys. Rev. C **74**, 014316 (2006).
[6] P. M. Walker and G. D. Dracoulis, Hyperfine Interact. **135**, 83 (2001).
[7] P. Chowdhury *et al.*, in Proceedings of the DAE Symp. on Nucl. Phys. **55**, 13 (2010), www.sympnp.org/proceedings.
[8] R.-D. Herzberg and D. M. Cox, Radiochim. Acta **99**, 441 (2011).
[9] A. Sobiczewski and K. Pomorski, Prog. Part. Nucl. Phys. **58**, 292 (2007).
[10] J. F. Berger *et al.*, Nucl. Phys. **685**, 1c (2001).
[11] M. Bender, K. Rutz, P.-G. Reinhard, J. A. Maruhn, and W. Greiner, Phys. Rev. C **60**, 034304 (1999).
[12] A. Ghiorso *et al.*, Phys. Rev. C **7**, 2032 (1973).
[13] R.-D. Herzberg *et al.*, Nature (London) **442**, 896 (2006).
[14] S. K. Tandel *et al.*, Phys. Rev. Lett. **97**, 082502 (2006).
[15] B. Sulignano *et al.*, Eur. Phys. J. A **33**, 327 (2007).
[16] A. P. Robinson *et al.*, Phys. Rev. C **78**, 034308 (2008).
[17] P. Chowdhury *et al.*, in *Proceedings of the 3rd International Conference on Frontiers in Nuclear Structure, Astrophysics, and Reactions: FINUSTAR 3, Rhodes, Greece*, edited by P. Demetriou, R. Julin, and S. Harissopulos, AIP Conf. Proc. 1377 (AIP, Melville, NY, 2010), pp. 13–17.
[18] L. G. Multhauf *et al.*, Phys. Rev. C **3**, 1338 (1971).
[19] K. Katori, I. Ahmad, and A. M. Friedman, Phys. Rev. C **78**, 014301 (2008).
[20] P. T. Greenlees *et al.*, Phys. Rev. C **78**, 021303 (2008).
[21] J. F. Berger, M. Girod, and D. Gogny, Comput. Phys. Commun. **63**, 365 (1991); J. Dechargé and D. Gogny, Phys. Rev. C **21**, 1568 (1980).
[22] J.-P. Delaroche *et al.*, Nucl. Phys. A **771**, 103 (2006).
[23] P. H. Heenen (private communication).
[24] R. V. Jolos, L. A. Malov, N. Yu. Shirikova, and A. V. Sushkov, J. Phys. G **38**, 115103 (2011).
[25] M. Leino *et al.*, Nucl. Instrum. Methods B **99**, 653 (1995).
[26] R. D. Page *et al.*, Nucl. Instrum. Methods B **204**, 634 (2003).
[27] L. Arnold *et al.*, IEEE Trans. Nucl. Sci. **53**, 723 (2006).
[28] I. Lazarus *et al.*, IEEE Trans. Nucl. Sci. **48**, 567 (2001).
[29] P. Rahkila, Nucl. Instrum. Methods Phys. Res. A **595**, 637 (2008).
[30] A.-P. Leppanen *et al.*, Eur. Phys. J. A **28**, 301 (2006).
[31] B. Sulignano, Ph.D. thesis, University of Mainz, 2007.
[32] N. Nica, Nucl. Data Sheets **106**, 813 (2005).
[33] G. D. Jones, Nucl. Instrum. Methods Phys. Res. A **488**, 471 (2002).
[34] K.-H. Schmidt *et al.*, Eur. Phys. J. A **8**, 141 (2000).
[35] H. Bartsch, K. Huber, U. Kneissl, and H. Sattler, Nucl. Instrum. Methods **121**, 185 (1974).
[36] S. Antalic *et al.*, Eur. Phys. J. A **47**, 301 (2011).
[37] R.-D. Herzberg *et al.*, Phys. Rev. C **65**, 014303 (2001).
[38] J. A. Becker *et al.*, Phys. Rev. C **41**, R9 (1990).
[39] J. E. Draper *et al.*, Phys. Rev. C **42**, R1791 (1990).
[40] S. M. Harris, Phys. Rev. **138**, B509 (1965).
[41] C. S. Wu, J. Y. Zeng, Z. Xing, X. Q. Chen, and J. Meng, Phys. Rev. C **45**, 261 (1992).
[42] S. Cwiok *et al.*, Comput. Phys. Commun. **46**, 379 (1987); W. Nazarewicz, J. Dudek, R. Bengtsson, T. Bengtsson, and I. Ragnarsson, Nucl. Phys. A **435**, 397 (1985).
[43] C. J. Gallagher, Phys. Rev. **126**, 1525 (1962).
[44] A. Bohr and B. R. Mottelson, *Nuclear Structure*, Vol. II (Benjamin, New York, 1969).
[45] E. Parr *et al.*, Eur. Phys. J. A (to be published).
[46] K. E. G. Löbner, Phys. Lett. B **26**, 369 (1968).
[47] U. Shirwadkar *et al.* (private communication); U. Shirwadkar, Ph.D. thesis, University of Massachusetts Lowell, 2009.
[48] A. V. Afanasjev, T. L. Khoo, S. Frauendorf, G. A. Lalazissis, and I. Ahmad, Phys. Rev. C **67**, 024309 (2003).
[49] M. Bender, P. Bonche, T. Duguet, and P.-H. Heenen, Nucl. Phys. A **723**, 354 (2003).
[50] M. Girod, J. P. Delaroche, J. F. Berger, and J. Libert, Phys. Lett. B **325**, 1 (1994).
[51] H. Dancer, Ph.D. thesis, Lyon 1, 2000, http://hola.univ-lyon1.fr/.
[52] L. D. Landau, Phys. Z. Sowjetunion **1**, 88 (1932); **2**, 46 (1932) [English translation in *Collected Papers of L. D. Landau* (Pergamon, New York, 1965)]; C. Zener, Proc. R. Soc. London A **137**, 696 (1932).
[53] B. Singh, R. Zywina, and R. B. Firestone, Nucl. Data Sheets **97**, 241 (2002).
[54] S. W. Yates *et al.*, Phys. Rev. C **12**, 442 (1975).
[55] V. G. Soloviev and T. Siklos, Nucl. Phys. **59**, 145 (1964).
[56] Y.-S. Chen, Y. Sun, and Z.-C. Gao, Phys. Rev. C **77**, 061305 (2008).
[57] R. F. Casten, W.-T. Chou, and N. V. Zamfir, Nucl. Phys. A **555**, 563 (1993).
[58] S. Peru, G. Gosselin, M. Martini, M. Dupuis, S. Hilaire, and J.-C. Devaux, Phys. Rev. C **83**, 014314 (2011).
[59] T. Nakatsukasa, K. Matsuyanagi, S. Mizutori, and Y. R. Shimizu, Phys. Rev. C **53**, 2213 (1996).
[60] J. Kvasil, N. Lo Iudice, F. Andreozzi, F. Knapp, and A. Porrino, Phys. Rev. C **75**, 034306 (2007).